

The Tsallis Entropy and the BKT-like Phase Transition in the Impact Parameter Space for pp and $\bar{p}p$ Collisions

S.D. Campos,^{*} V.A. Okorokov,[†] and C.V. Moraes^{*}

^{*}*Departamento de Física, Química e Matemática,
Universidade Federal de São Carlos, 13052-780, Sorocaba, SP, Brazil and*

[†]*National Research Nuclear University MEPhI (Moscow Engineering
Physics Institute), Kashirskoe highway 31, 115409 Moscow, Russia*

(Dated: December 3, 2019)

In this paper, one uses the Tsallis entropy in the impact parameter space to study pp and $\bar{p}p$ inelastic overlap function and the energy density filling up mechanism responsible by the so-called black disk limit as the energy increases. The Tsallis entropy is non-additive and non-extensive and these features are of fundamental importance since the internal constituents of pp and $\bar{p}p$ are strongly correlated and also the existence of the multifractal character of the total cross-section. The entropy approach presented here result in a phase transition occurring inside the hadrons as the energy increases. This phase transition in the impact parameter space is quite similar to the Berezinskii–Kosterlitz–Thouless phase transition, possessing also a topological feature due to the multifractal dimension of the total cross-sections in pp and $\bar{p}p$ scattering. The transition temperature is calculated, revealing a negative sign in some energy regimes. This qualitative result corroborates some recent theoretical results.

PACS numbers: 13.85.Dz;13.85.Lg

I. INTRODUCTION

The transition point separating two different states of matter is known as a phase transition and is observed when a physical system suddenly changes its macroscopic behavior due to a smooth variation of the order parameter passing through its critical value. In the classical point of view, the temperature is usually the driving parameter of such transitions and determines exactly the phase transition by heat transfer. Both the superfluid helium and the Ginzburg–Landau superconducting model are very well-known examples where phase transitions are thermal-dependent in the classical sense. In the quantum world at zero temperature, the tuning parameter is chosen depending on the experiment (for instance, the magnetic field, chemical potential or electric field), and in these systems, the phase transition is known as the quantum phase transition [1].

In a modern view, phase transitions (classical or quantum) are classified as first-order or second-order. The first-order phase transition is determined by the discontinuity at first derivative of a relevant thermodynamic potential and, as consequence, such phase transition can also be called as discontinuous one, from the point of view of the behavior for the first derivative of the thermodynamic potential. The second-order phase transition is continuous at the first derivative and divergent at higher order derivatives, and such phase transition can also be called as continuous one. Despite the significant progress in the study of critical phenomena there some disagreements with regard to terminology. For instance, the classification of phase transitions as first-order or continuous is justified in [2]. However, such classification seems self-contradictory because uses different categories, namely, "order" and the feature (continuity/discontinuity) in the behavior of the first derivative of a relevant thermodynamic potential. Therefore the well-known classification as first- /second-order [3] is used for phase transitions in this paper. In any classification, the so-called critical point separates the system ordering from a symmetric state to a broken-symmetry state.

The Berezinskii–Kosterlitz–Thouless (BKT) phase transition [4, 5], whose main goal is the study of correlations between pairs of topological defects (vortex-antivortex), is an example from a geometrical point of view. In condensed matter physics, the study of such transition is a tool to understand how collective coherent phenomena (a topological defect) can emerge from certain structures and how it can be connected to another one in a different space. If the interaction between topological defects depends on the logarithm of the spatial separation, then the BKT phase transition takes place being used to explain the phenomenon. As will show later, the model proposed here presents a BKT-like phase transition.

^{*}Electronic address: sergiadc@ufscar.br

[†]Electronic address: VAOkorokov@mephi.ru; Okorokov@bnl.gov

As well-known, phase transitions are closely connected to the entropy of a system and to the Helmholtz free energy, which is nothing more than the useful work that can be extracted from a closed thermodynamic system at a constant temperature. In general, one applies the Boltzmann entropy (extensive) to this kind of systems. However, a non-extensive form of entropy based on the q -Gaussian was proposed and successfully used to calculate and explain some physical properties in several systems, in particular, those with fractal properties. This is the so-called Tsallis entropy (TE) [6]. Notice that in the last decades, various approaches have been used to calculate the entropy of systems, presenting interesting properties. The Shannon entropy [7], the Rényi entropy [8], and the von Neumann entropy [9] are examples of such calculation approaches, each one applied to a specific physical problem. However, all these formulations can be reduced to the TE [10].

Entropy is one of the most important physical quantities in thermodynamics and cannot be put aside in any reliable model, even when its results are disconcerting in the classical world [11]. Moreover, entropy cannot only be viewed as the disorder of a given system. Since the fundamental work of Shannon [7], the entropy have been also related to the amount of information we can attain from the system. It should be stressed that the applicability of such quantity as "entropy" for the study of an interaction process between atomic nuclei and particles requires a detailed and rigorous justification. Here one can note the following with regard of two main problems: (i) a finite number of particles in the system under consideration and (ii) \mathcal{T} invariance in the quantum field theory (QFT). First of all, the usual way to use entropy is by assuming some large statistical ensemble (canonical, for instance). In the classical view, the number of elements in such an ensemble is at least of the order of the Avogadro number. However, there are filtering methods used in information theory to reduce the number of bits, allowing at least an estimation to the entropy. Then, the size of the ensemble is not a problem, at first glance. Of course, if the size of the ensemble grows, then the estimation may also tend to a "better" value [12]. Second, indeed, the entropy almost always grows. Nevertheless, there are some systems where the entropy achieves negative values. The concept of negative absolute temperature can be applied in such systems [11]. In these systems, the arrow of time is the same, but a non-trivial interpretation must be used to explain the result. So, the \mathcal{T} invariance of the QFT is preserved and, in particular, the strong interactions are in a safe place.

The calculation of the entropy is a complicated task but can provide remarkable results as the proton and electron radii in the nucleus [13]. The z -scaling also can be used to furnish the entropy in a system with particle production [14] and further be calculated in D -branes [15]. All these approaches used to evaluate the entropy reveal some particular thermodynamics aspect of the system under study.

Recently, the concept of fractal dimensions was introduced in the study of pp and $\bar{p}p$ total cross sections [16, 17]. These fractal dimensions were used to explain the transition from a decreasing total cross section for an increasing one as the energy tends to infinity. The fractal dimensions emerging in these pictures are energy-dependent. On the other hand, in terms of momentum space (or in configuration space), an attempt to connect the intermittency pattern [18, 19] in hadronic collisions to fractal dimensions uses a second-order phase transition [20–23]. The approach presented in [24] shows this possibility through the use of thermofractals.

In the present paper, is proposed a naive model to evaluate the entropy of pp and $\bar{p}p$ elastic scattering adopting subtleties assumptions. These assertions allow the connection of the TE and the inelastic overlap function in the impact parameter space, providing a novel interpretation of the energy density filling up mechanism of the hadron as the collision energy increases. This process can enhance the understanding of how the black disk limit is achieved (or not).

The paper is organized as follows. In section II only the essential of the TE is presented. In section III the impact parameter space is used as the background to the development of the model. Section IV present a basic example of an application using the most general experimental results and phenomenological approaches to the inelastic overlap function. Section V presents critical remarks about the results.

II. THE TSALLIS ENTROPY

Although entropy is a well-defined quantity in physics its calculation depends on the presence or not of correlations among the components of the lattice, for instance. The internal structure of the hadron grows in complexity as the energy increases, possibly showing a black disk picture as $s \rightarrow \infty$, where s is the squared-energy in the center-of-mass system (cms). This result prevents the use of the Boltzmann entropy since the correlation between the constituents of the hadron grows as s increases due to the confinement potential. Accordingly, the use of the TE may furnish a better understanding of the internal structure of the hadron than the Boltzmann one.

Note that the Boltzmann entropy (S_B) assumes each part of the lattice as an independent system with a defined entropy, and the sum of all cells results in the total entropy of the system. Then, this entropy is additive, i.e., for a system composed of a countable number of subsystems $i = 1, 2, \dots, W$ each one with entropy S_i the total entropy is

given by

$$S_B = \sum_{i=1}^W S_i. \quad (1)$$

Indeed, if the subsystems have no correlations at all or only local correlations, then S_B is also extensive [6]. However, if there are correlations between the cells the Boltzmann entropy is no longer valid and the entropy of each cell cannot be computed separately and consequently, the total entropy is not the sum of each cell of the lattice. Of course, if the correlations are weak, then the Boltzmann entropy can be used as a first approximation to solve the problem. An alternative approach, however, which takes into account the correlations is provided by the TE (S_T) [6]. In a single system composed of two subsystems a and b it is written as

$$S_T = S_a + S_b + (1 - w)S_a S_b, \quad (2)$$

where w is the entropic index. If $w \neq 1$, then S_T is non-additive as well as non-extensive. On the other hand, if $w = 1$, the TE is reduced to the Boltzmann entropy one. Thus, w characterizes the degree of non-extensivity of the system. It is important to stress this kind of entropy calculation is applicable when the system exhibits some long-range correlations, intrinsic fluctuations or fractal structure in phase space [25]. The continuous form of the TE is given by [26]

$$S_T(p, w) = \frac{1}{w - 1} \left(1 - \int_{-\infty}^{\infty} [p(x)]^w dx \right), \quad (3)$$

where $p(x)$ is the probability density function. The existence of fractal structures in the momentum and in the energy space for both pp and $\bar{p}p$ collisions may allow the use of the TE to study how these fractal dimensions can contribute to the understanding of the collision process. Additionally, if one looks to the entropy as the information that may be gained observing a physical quantity depending on (s, b) in the impact parameter space, then b may be used as a measure of this information and how it acts on the black disk picture.

III. IMPACT PARAMETER POINT OF VIEW

The impact parameter space is the right place to study the fractal behavior of pp and $\bar{p}p$ since it allows a general view of the elastic and inelastic channels of the scattering. In this way, using the impact parameter formalism, the fractal dimensions obtained in [16, 18–23] may be viewed as a consequence of a phase transition in pp and $\bar{p}p$ elastic scattering whose geometric picture may also indicates a geometric phase transition. This topological phase transition taking place inside the hadron may be responsible be a change in the energy density filling up mechanism, allowing the emergence of fractal structures in the total cross section.

The impact parameter is very useful as a geometrical view of the scattering process. The squared momentum transfer $-t = |t|$ is replaced by its conjugate variable b , i.e., the transverse distance between the colliding particles in impact parameter space. Is this space the analytical function $F(s, t) = \text{Re}F(s, t) + i\text{Im}F(s, t)$ representing the elastic scattering is written at fixed s as

$$F(s, t) = i4\pi s \int_0^\infty db b J_0(b\sqrt{|t|}) \Gamma(s, b) = i4\pi s \int_0^\infty db b J_0(b\sqrt{|t|}) \{1 - \exp[i\chi(s, b)]\}, \quad (4)$$

where $J_0(x)$ is a zeroth order Bessel function, $\Gamma(s, b) = \text{Re}\Gamma(s, b) + i\text{Im}\Gamma(s, b) = 1 - \exp[i\chi(s, b)]$ is the profile function and $\chi(s, b)$ is the eikonal function written as $\chi(s, b) = \text{Re}\chi(s, b) + i\text{Im}\chi(s, b)$. The unitarity condition connects the total (σ_{tot}), elastic (σ_{el}) and inelastic (σ_{in}) cross sections to the profile function and can be written in b -representation as

$$2\text{Re}\Gamma(s, b) = |\Gamma(s, b)|^2 + G_{\text{inel}}(s, b), \quad (5)$$

where $G_{\text{inel}}(s, b)$ is the real function called inelastic overlap one [27] and $|\Gamma(s, b)|^2$ represents the shadow contribution of the elastic channel, i.e.

$$\sigma_{\text{tot}}(s) = 2 \int d^2b \text{Re}\Gamma(s, b), \quad \sigma_{\text{el}}(s) = \int d^2b |\Gamma(s, b)|^2, \quad \sigma_{\text{in}}(s) = \int d^2b G_{\text{inel}}(s, b). \quad (6)$$

Here it is used the optical theorem $s^{-1}\text{Im}F(s, 0) = \sigma_{\text{tot}}(s)$ [28, 29]. Also the unitarity condition demands $\text{Im}\chi(s, b) \geq 0$, implying that $G_{\text{inel}}(s, b)$ represents the probability of an elastic scattering in the 2D kinematic space (s, b) and this quantity is given by [30]

$$G_{\text{inel}}(s, b) = 1 - \exp[-2\text{Im}\chi(s, b)] \leq 1. \quad (7)$$

As usual, one can introduce the opacity $\Omega(s, b)$ defined as $\Omega(s, b) = 2\text{Im}\chi(s, b)$. It is well-known that the opacity is a measure of the matter density distribution inside the incident particles. At lower energies [31], the opacity presents a Gaussian shape not observed in LHC data, whose indication is the growth of opacity at small b as presented in TOTEM data [32]. The inelastic profile function, on the other hand, determines how absorptive is the interaction region (inelastic) depending on b . When $G_{\text{inel}}(s, b) = 0$ the object is said transparent and to $G_{\text{inel}}(s, b) = 1$, the absorption is maximal. Theoretically the latter result, in general, occurs at $b = 0$ fm in the asymptotic condition $s \rightarrow \infty$. Notwithstanding, in [33, 34] there is an approach indicating that at $b = 0$ fm, the black disk limit is not achieved. Indeed, the black disk picture seems to be achieved at some critical b_c , near forward direction, indicating the arising of a gray area [33, 34]. This model was further analyzed in [35–42] resulting in the so-called hollowness effect near the forward direction.

Using the Fourier–Bessel transform of the amplitude (4) one can write the dimensionless profile function as

$$\Gamma(s, b) = \frac{-i}{8\pi} \int_0^\infty d|t| J_0(b\sqrt{|t|}) \frac{F(s, t)}{s} \equiv \frac{-i}{8\pi} F(s, b). \quad (8)$$

One can suggest that the t -dependence is taken into account by the one real function $f(s, t)$ which is common for both the real and imagine part of the amplitude $F(s, t)$, i. e. $\text{Re}F(s, t) = \text{Re}F(s, 0)f(s, t)$ and $\text{Im}F(s, t) = \text{Im}F(s, 0)f(s, t)$. These relations imply $f(s, 0) = 1$. Then

$$\text{Re}\Gamma(s, b) = \frac{1}{8\pi} \frac{\text{Im}F(s, 0)}{s} \int_0^\infty d|t| J_0(b\sqrt{|t|}) f(s, t) = \frac{\sigma_{\text{tot}}}{8\pi} f(s, b), \quad (9a)$$

$$\text{Im}\Gamma(s, b) = -\frac{1}{8\pi} \frac{\text{Re}F(s, 0)}{s} \int_0^\infty d|t| J_0(b\sqrt{|t|}) f(s, t) = -\rho \frac{\sigma_{\text{tot}}}{8\pi} f(s, b) \equiv -\rho \text{Re}\Gamma(s, b), \quad (9b)$$

where $\rho(s) \equiv \text{Re}F(s, 0)/\text{Im}F(s, 0)$ is the the ratio of the real to imaginary part of the amplitude in the forward direction. It should be noted that experimental data show $|\rho(s)| \lesssim 0.3$ (0.2) at $\sqrt{s} \gtrsim 5$ (3) GeV for pp ($\bar{p}p$) collisions. Therefore one can neglect the $\text{Re}F(s, t)$ with respect of the $\text{Im}F(s, t)$ and, as consequence, the $\text{Im}\Gamma(s, b)$ with respect of the $\text{Re}\Gamma(s, b)$ at accuracy level not worse than 0.3 (0.2) in the energy domains indicated above for pp and $\bar{p}p$ collisions [17]. Based on the equations (9a) and (9b) one can derive for the inelastic overlap function

$$\begin{aligned} G_{\text{inel}}(s, b) &= \text{Re}\Gamma(s, b) \{2 - \text{Re}\Gamma(s, b)[1 + \rho^2(s)]\} \\ &\approx \text{Re}\Gamma(s, b) \{2 - \text{Re}\Gamma(s, b)\}, \end{aligned} \quad (10)$$

where the approximate relation is valid at accuracy level not worse than 0.09 (0.04) in wide energy domain $\sqrt{s} \gtrsim 5$ (3) GeV for pp ($\bar{p}p$) collisions.

It should be noted that the results obtained above are derived with help of the most general property of quantum field theory, namely, unitarity condition and consequently they are model independent.

A. Tsallis Entropy in the Impact Parameter Space

In order to use the TE in the impact parameter space one assumes the following assumptions:

1. the probability density function is calculated inside a disk of radius b , the impact parameter;
2. the entropic index w can be replaced by a single real evaluated function $w = w(s/s_c) \geq 0$, where s_c is the critical point associated to the phase transition occurring in the total cross section [16].

The first assumption is necessary to establish an ordering in the elastic scattering process considering the growth of the black disk picture as s increases. In the impact parameter space, all functions are b -dependent (fixed- s) and at each value of s ($s_1 < s_2 < \dots < s_n$), the description of the elastic scattering acquires a clear black disk behavior as shown by the profile function and the inelastic overlap function [30], i.e., the hadron radius grows with the energy.

Then, at each s_i there is a maximum value to $\text{Re}\Gamma(s_i, b = 0)$, for instance, with an effective maximum range (or radius) b_i ($i = 1, 2, \dots, n$). Hence, one computes the amount of information inside the disk of radius b_i .

The second assumption is related to the critical point where the phase transition takes place. According to [16], there are two fractal dimensions in the total cross section experimental dataset to pp and $\bar{p}p$. The energy range where $\sigma_{\text{tot}}(s)$ change its curvature is $\sqrt{s} \sim 10 - 30$ GeV, depending on the dataset considered (pp or $\bar{p}p$). The non-extensivity of the system is given by s/s_c and it represents a measure of the correlations among the internal constituents of pp and $\bar{p}p$. The phase transition occurring in the total cross section at s_c represents a break in the symmetry predicted in the seminal paper [43] and, before that, in the [44].

These assumptions can provide a way to calculate the entropy generated due a phase transition in the total cross section as s increases [16]. In order to do that, the integral in (3) is rewritten assuming the collision event inside a disk of radius $b > 0$ and an entropic index s/s_c

$$1 - \int_0^\infty [p(b')]^{s/s_c} db' = 1 - \int_0^b [p(b')]^{s/s_c} db' = m[1 - nG_{\text{inel}}(s, b)], \quad (11)$$

where m, n are dimensionless free parameters. In order to prevent complex values to the entropy one imposes m and n are real. Although the concept of complex entropy can be well-defined in information theory [45], it will be developed in particle scattering elsewhere. Because the $P(s, b) = \int_0^b [p(b')]^{s/s_c} db'$ is some probability and $0 \leq P(s, b) \leq 1$ then $0 \leq n \leq G_{\text{inel}}^{-1}(s, b)$. It is important to stress that the upper limit in the integration acts as a cutoff in the impact parameter space. This cannot be viewed as a limitation of the method since it is expected that $b \rightarrow \infty$, all functions b -dependent vanishing. Hence, contributions above some b can be neglected assuming an effective range of interaction. Therefore, the TE can be written in terms of the inelastic overlap function as ($k \equiv s/s_c - 1$)

$$\begin{aligned} S_T(s, b) &= mk^{-1}[1 - nG_{\text{inel}}(s, b)] = mk^{-1}(1 - n\text{Re}\Gamma(s, b)\{2 - \text{Re}\Gamma(s, b)[1 + \rho^2(s)]\}) \\ &\approx mk^{-1}(1 - n\text{Re}\Gamma(s, b)\{2 - \text{Re}\Gamma(s, b)\}). \end{aligned} \quad (12)$$

The relations can be rewritten as follows

$$S_T(s, b) = mk^{-1}[\text{Re}\Gamma(s, b) - X_1][\text{Re}\Gamma(s, b) - X_2], \quad (13)$$

where $X_i = [1 + \rho^2(s)]^{-1}(1 \pm \sqrt{1 - [1 + \rho^2(s)]/n}) \approx 1 \pm \sqrt{1 - 1/n}$, $i = 1, 2$. Note that m and n rules as scales for the problem and does not alter the physical interpretation of any result obtained below, unless $0 \leq n < 1$, where $\forall i = 1, 2 : X_i$ - complex and the concept of complex entropy arises. Thus, for the sake of simplicity, one adopts $n = 1$ and $m = 1$ allowing the TE assumes its symmetric form in the limiting case $\rho \rightarrow 0$

$$\begin{aligned} S_T(s, b) &= k^{-1}[1 - G_{\text{inel}}(s, b)] = k^{-1}(1 - \text{Re}\Gamma(s, b)\{2 - \text{Re}\Gamma(s, b)[1 + \rho^2(s)]\}) \\ &\approx k^{-1}[1 - \text{Re}\Gamma(s, b)]^2. \end{aligned} \quad (14)$$

The above result furnishes a measure of the entropy in the impact parameter space through the use of the inelastic overlap function. The signature (positive or negative) of the TE reveals an s -dependence analyzed as follows. Considering $s < s_c$, the signature of S_T is negative and it can be interpreted as the system using the energy of the beam to self-organize or maintain its internal structure (quarks and gluons). Then, as s increases the entropy tends to a maximum by negative values, i.e., the system tends to achieve the maximum of its self-organization as well. Moreover, as observed in [16], the fractal dimension in this energy range is negative and different to pp and $\bar{p}p$, producing distinct patterns to $G_{\text{inel}}(s, b)$. Hence, the measure of the emptiness of pp and $\bar{p}p$ total cross section results in different values to S_T .

The negative entropy and the negative fractal dimensions imply the constituents, the internal arrangement to pp and $\bar{p}p$ are unlike, i.e., the quark-quark and quark-gluon arrangement of the proton are different of the antiquark-antiquark and antiquark-gluon arrangement of the antiproton. In the popular picture, one says that the odderon distinguishes particle from antiparticle.

When the energy s grows and go through the transition point s_c , the TE turns positive and stands for the growing disorder in the system. As obtained in [16], the total cross section to pp and $\bar{p}p$ possesses positive fractal dimensions to $s > s_c$ and both tends to the same value as $s \rightarrow \infty$. Both results have shown that at high energies the arrangement of the internal constituents to pp and $\bar{p}p$ tends to the same behavior. Then, the pomeron does not distinguish particle from antiparticle.

The different internal arrangement of proton and antiproton may absorb the incoming energy by distinct mechanisms. As pointed out [16], the negative fractal dimension represents the emptiness of the hadron internal arrangement

and the total cross section is a measure of that. The internal arrangement of quarks and gluons at lower energies in the proton picture is less empty than the arrangement of the antiquarks and gluons inside the antiproton, as can be viewed in the total cross section experimental dataset to $s < s_c$.

At the transition point, ($s = s_c$) the fractal dimension to pp and $\bar{p}p$ total cross section is null and the system achieves its maximum capability to convert the absorbed energy in order. This point may indicate the first saturation point in pp and $\bar{p}p$ total cross section dataset. It is interesting to note that pp and $\bar{p}p$ total cross section tends to the same saturation point s_c , possibly indicating this value as a universal character of total cross sections.

Above the critical point, ($s > s_c$), the internal constituents of pp and $\bar{p}p$ achieve degrees of freedom previously blocked by using the energy coming from the beam converted in thermal agitation resulting in the rise of the total cross-section as s increases.

The above scenarios introduced by the TE and by the concept of fractal dimension result in the question of how occurs the filling up mechanism responsible by the black disk behavior of pp and $\bar{p}p$ as $s \rightarrow \infty$. A possible answer is given as follows. As well-known, in QCD the confinement of quarks and gluons prevent its freedom below the Hagedorn temperature [46], where the hadrons are no longer stable. However, the increasing energy of the scattering imply in the enhanced of the thermal bath at each particle is subject. This energy is then transferred to the internal constituents of the proton and antiproton by a heat transport mechanism.

The zero entropy state can be established when at $nG_{\text{inel}}(s, b) = 1$ to some particular (s, b) . As well-known, zero entropy occurs when a system achieves its ground-state (or its maximum self-organization state). Thus, at this point, the physical state of the system is completely known (the ways one can arrange its internal configuration is exactly one). The general belief is that $nG_{\text{inel}}(s, b) = 1$ is achieved in the asymptotic limit $s \rightarrow \infty$ and at $b = 0$. Then, from some s sufficiently high the energy of both pp and $\bar{p}p$ possess the same behavior at $b = 0$. However, there exist some models indicating this result may be achieved at some $b \neq 0$ [35, 47]. The implication of that is the appearance of a gray area in the inelastic overlap function near $b = 0$.

It is interesting to note that the first equation in the chain (12) can also be written assuming only as the first order of the logarithm expansion below

$$S_T(s, b) = -mk^{-1} \ln[nG_{\text{inel}}(s, b)], \quad (15)$$

implying the higher orders are corrections to equation (12). In addition, if the logarithm of the inelastic overlap function is connected to the spatial separation of the pair of the constituents of the hadron, then it can represent the interaction of topological defects [4, 5] inside the hadron. Therefore, the TE given by the equation (15) may be interpreted as a BKT-like phase transition occurring inside the hadron at s_c .

B. Phase Transition at the Critical Temperature

The approach of the total internal energy U by *effective* potential V and approximate relations for the Coulomb (V_C) and confinement (V_c) potentials in the (s, b) space are considered in detail elsewhere [48]. Within potential approach one can use the following general equation

$$T(s, b) = V(s, b)/S_T(s, b). \quad (16)$$

which corresponds to the Helmholtz free energy [49].

Due the modifications [48], the Coulomb potential $V_C(s, b) = -ab^{-3}(b^2 - 2/s)$ presents a physical root in the impact parameter space given by

$$b_0 = \sqrt{2/s} \quad (17)$$

with a natural shrinkage as s increases, where $a > 0$ is a dimensionless parameter corresponding to the electrostatic interaction of the pair. Considering finite energies, this root is never reached, since it is below the $b_{\text{min}} = \sqrt{6/s}$ at which the $V_C(s, b)$ is minimum. The temperature of the process with Coulomb potential can be written as follows

$$T(s, b) = \frac{-kab^{-3}(b^2 - 2/s)}{m[1 - nG_{\text{inel}}(s, b)]}. \quad (18)$$

The above root is also given by (17) and is never reached. However, the sign of the temperature depends on the range of energy considered. If $s < s_c$, the temperature is positive and, if $s > s_c$, the temperature is negative. In this picture, to energies below s_c , the hadrons (point-like particles) tend to occupy different temperatures. However, above the critical value, they tend to the same energy, as revealed by the negative temperature.

The temperature must be normalized to obey the unitarity condition. On the other hand, the relevant information here is the sign of the temperature, depending on s , since this approach (the use of the effective potential) does not allow the precise knowledge of the critical temperature. Hence, normalizing the temperature one still maintain the relevant information about its sign only by using the procedure

$$\tilde{T}(s, b) = \begin{cases} +1, & \text{if } s < s_c \\ -1, & \text{if } s > s_c \end{cases} \quad (19)$$

The QCD critical point in the temperature-density phase diagram indicates the separation from a confined to a non-confined state and it defines a first-order phase transition (symmetry breaking). On the other hand, the QCD critical point belongs to the 3d Ising universality class, which implies in a fractal dimension on the transverse momentum space [23]. Therefore, the phase transition occurring in the momentum space is caused by a symmetry breaking as pointed out in the thermofractal approach developed in [24].

The usual way is to define a certain order parameter to distinguish the confined and non-confined phases. The Polyakov loop and the chiral condensate are attempts to solve this problem [50]. The first one is applicable when the internal constituents of the hadron are not taken into account (without quarks). To the second one, the quarks are important to characterize the breaking of the flavor symmetry. As noted in [50], the order parameter available in the Polyakov loop is the correlator which is non-local and this situation is similar to the BKT phase transition in 1D systems, where the correlator changes its behavior at large distances [4, 5]. The BKT phase transition in 2D systems needs the vortex-antivortex pair to evaluate the transition temperature where the symmetry-breaking occurs. Moreover, it is of fundamental importance that interactions between the pairs fall off at large distances as r^{-2} whose consequence is that dislocation depends logarithmically on the size of the system [5]. Unfortunately, this result cannot remain valid inside pp or $\bar{p}p$ since quarks and gluons obey the QCD confinement rule whose potential presents some interesting characteristics resulting the phase transition obtained here is a BKT-like phase transition.

To set the problem one start by considering the approximation of the confinement potential in the (s, b) space [48]: $V_c(s, b) = -4\alpha_s(\eta s)/3\varepsilon_2 b + \kappa\varepsilon_2 b$, where $\alpha_s(\mu)$ is the running coupling constant of the strong interaction at a specific energy scale μ [51], κ – string tension, $\eta = \mu/s = 1/9$, $\varepsilon_2 = r/b \leq 1$, r is the spatial separation of the pair, strictly speaking, the infinitely heavy (static) quarks and antiquarks inside the hadron. The zero of the confinement potential is given by [48]

$$b_0 = \varepsilon_2^{-1} \sqrt{\zeta} \propto \sqrt{\alpha_s(\eta s)}, \quad \zeta \equiv 4\alpha_s(\eta s)/3\kappa, \quad (20)$$

where the allowable ranges are taken into account for linear scales r and b , i.e. $r, b > 0$. Of course, b_0 is a decreasing function of s entailing the shrinkage of b_0 as $s \rightarrow s_c$ and also when $s \rightarrow \infty$. Also note that at $s = s_c$ one gets the critical value $b_0 = b_c$ which determines in the impact parameter space a critical point related to the critical point in the energy variable as shown in [16]. The temperature to a fixed- s can be easily obtained

$$T(s, b) = \frac{k(-4\alpha_s(\eta s)/3\varepsilon_2 b + \kappa\varepsilon_2 b)}{m[1 - nG_{\text{inel}}(s, b)]}. \quad (21)$$

which present a zero given also by (20). The thermalization can take place if the characteristic timescale for exchange energy between particles and between the beam and the particles must be shorter than the time scale to heat and loss, implying that process needs high collisions rate. The sign of the temperature depends on s and b relate to s_c and b_0 , respectively. We are not interested here in the precise calculation of the temperature, as the preceding subsection. Indeed, the physical interesting result obtained is the occurrence of a change of sign of the temperature, since it is related with the energy occupation states inside the hadron. Considering only the changes in the sign of the temperature, one can normalize it by using

$$\tilde{T}(s, b) = \begin{cases} s < s_c & \begin{cases} +1, & \text{if } b < b_0 \\ -1, & \text{if } b > b_0 \end{cases} \\ s > s_c & \begin{cases} -1, & \text{if } b < b_0 \\ +1, & \text{if } b > b_0 \end{cases} \end{cases} \quad (22)$$

The above normalization procedure retains the information about the sign, resulting in the knowledge of the energy occupation states and defining the phase transition occurring inside the hadron as the energy increases passing through s_c .

As seen the sign of the above result depends on values of s and b with respect to s_c and b_0 . Mathematically speaking, the only requirement to obtain a negative temperature is that the entropy should not be restricted to monotonically increasing of the internal energy U [52]. Its physical meaning is also well-defined: the occupation distribution is

inverted, where high-energies states are populated more than low-energies states. The occupation probability of a quantum state increases exactly with the energy of the state.

The two situations depending on s and b are analyzed as follows. If $s < s_c$, the temperature is positive to $b < b_0$, indicating the constituents does not possess a well-defined structure due the quarks and gluons are distributed in different energy states. On the other hand, the region $b > b_0$ possess a well-defined structure since the constituents are in the higher-energy occupation states due the negative temperature. Now, if $s > s_c$ the temperature possess the opposite behavior and the higher-energy states occupy the region below b_0 .

The shrinkage of b_0 as $s \rightarrow s_c$ shows a diminishing value of the emptiness of the hadron as indicated the slow down in the total cross section experimental data in this energy range. At $s = s_c$ a phase transition takes place and the higher-energy occupation states change its place towards the center of the hadron. Now, the total cross section measures a well-defined structure located in the central region of the hadron. However, the shrinkage of b_0 is again observed tending slowly to zero as $s \rightarrow \infty$.

Whereas the energy of the beam is transferred to the hadron the higher-energy occupation grows in the negative temperature region. If the energy flows from the outside to inside the hadron one can suppose the higher-energy occupation number is located (a) far from $b_0 \ll b$ in the case $s < s_c$ and (b) near $b \approx b_0$ when $s > s_c$. The hadron picture in (a) is similar to a torus with a smooth edge toward the center. In (b) one has basically the same behavior but now the hadron seems like a disk where the center is less opaque than the region near b_0 indicating the appearance of a gray area [33, 34]. Moreover, b_0 shrinks to zero in the asymptotic limit, and the hadron tends to a point-like picture if no new phase transition occurs.

IV. BASIC APPLICATION: GENERAL FORM FOR THE OVERLAP FUNCTION

In this section one focus on recent inelastic overlap function models comparing results by using S_T here obtained. These comparisons may furnish a better understanding of how entropy is released in each model. There is a wide set of models for nucleon-nucleon elastic scattering. Therefore it seems reasonable the discussion of only models based on the most general and basic statements of the modern quantum theory. In the present paper, the (a) unitarity condition and (b) asymptotic theorems are basic ground.

A. Non-central collisions ($b \neq 0$)

The most general and well-established experimental result for elastic scattering is the rapid decreasing of the differential cross section ($d\sigma/dq^2$) with the increasing $|t| \simeq q^2$ in the diffraction peak. As a first approximation, the $d\sigma/dq^2$ shows exponential shape with slope $B(s)$ at q^2 under consideration. Thus, one writes for the t -dependent part of scattering amplitude $f(s, t) = \exp[B(s)|t|/2]$ and

$$f(s, b) = \int_0^\infty d|t| J_0(b\sqrt{|t|}) \exp\left[\frac{B(s)|t|}{2}\right] \approx 2 \int_0^\infty dq q J_0(bq) \exp\left[-\frac{B(s)q^2}{2}\right] = \frac{2}{B(s)} \exp\left[-\frac{b^2}{2B(s)}\right]. \quad (23)$$

Then

$$\text{Re}\Gamma(s, b) = [\sigma_{\text{tot}}/4\pi B(s)] \exp[-b^2/2B(s)] \equiv \zeta(s) \exp[-b^2/2B(s)], \quad (24a)$$

$$\text{Im}\Gamma(s, b) = [-\rho\sigma_{\text{tot}}/4\pi B(s)] \exp[-b^2/2B(s)] \equiv -\rho(s)\zeta(s) \exp[-b^2/2B(s)], \quad (24b)$$

where ζ is the parameter defined as following

$$\zeta(s) = \frac{\sigma_{\text{tot}}(s)}{4\pi B(s)} = \frac{4\sigma_{\text{el}}(s)}{[1 + \rho^2(s)]\sigma_{\text{tot}}(s)} \approx \frac{4\sigma_{\text{el}}(s)}{\sigma_{\text{tot}}(s)}. \quad (25)$$

Note that at $\zeta = 1$ the $G_{\text{inel}}(s, b)$ represent a black disk and to $\zeta \neq 1$ the inelastic overlap function diminishes. Moreover, the position of maximum $b_{\text{max}}^2 = 2B \ln \zeta$ with full absorption $G_{\text{inel}}(s, b_{\text{max}}) = 1$ depends on $B(s)$ and $\zeta(s)$.

Taking into account (10) and (12) one can deduce the final expressions for inelastic overlap function and Tsallis entropy respectively within general phenomenological way for scattering amplitude

$$\begin{aligned} G_{\text{inel}}(s, b) &= \zeta(s) \exp[-b^2/2B(s)] \{2 - \zeta(s) \exp[-b^2/2B(s)] [1 + \rho^2(s)]\} \\ &\approx \zeta(s) \exp[-b^2/2B(s)] \{2 - \zeta(s) \exp[-b^2/2B(s)]\}, \end{aligned} \quad (26)$$

$$\begin{aligned}
S_T(s, b) &= mk^{-1} (1 - n\zeta(s) \exp[-b^2/2B(s)] \{2 - \zeta(s) \exp[-b^2/2B(s)] [1 + \rho^2(s)]\}) \\
&\approx mk^{-1} (1 - n\zeta(s) \exp[-b^2/2B(s)] \{2 - \zeta(s) \exp[-b^2/2B(s)]\}).
\end{aligned} \tag{27}$$

For strong interaction processes, the temperature in the above model independent approach for the $G_{\text{inel}}(s, b)$ can be performed using (13), resulting the general case

$$T(s, b) = \frac{k(-4\alpha_s(\eta s)/3\varepsilon_2 b + \kappa\varepsilon_2 b)}{m[\text{Re}\Gamma(s, b) - X_1][\text{Re}\Gamma(s, b) - X_2]}, \tag{28}$$

where the symmetric form is written as

$$T(s, b) = \frac{k(-4\alpha_s(\eta s)/3\varepsilon_2 b + \kappa\varepsilon_2 b)}{[\text{Re}\Gamma(s, b) - 1]^2}. \tag{29}$$

The above result agrees with the analyzes performed in the preceding section showing the picture of the smoothed torus when $s < s_c$ and a disk-like if $s > s_c$ tending to a point-like particle in the asymptotic energy limit.

B. Central collisions ($b = 0$)

The general equations (26) and (27) are obtained assuming the most general phenomenological view for the differential cross section $d\sigma/dq^2 = [\text{Im}F(s, 0)/4\sqrt{\pi}s]^2 \exp[-B(s)q^2/2]$. However, the concrete form for the energy dependence of both the $G_{\text{inel}}(s, b)$ and the $S_T(s, b)$ is driven by the corresponding dependence for scattering parameters. The exact relations in (26), (27) are defined by energy dependencies for global scattering parameters σ_{tot} , ρ and for slope B , while the corresponding approximate relations depend on the ratio $R_{e/t} = \sigma_{\text{el}}/\sigma_{\text{tot}}$ and B . The forward condition $b = 0$ allows the exclusion of the dependence on $B(s)$. In this specific case, $\text{Re}\Gamma(s, 0) = \zeta(s)$ and $\text{Im}\Gamma(s, 0) = -\rho(s)\zeta(s)$. Considering exactly central collision with $b = 0$ one obtains from general relations (26), (27) the following equations:

$$G_{\text{inel}}(s, 0) = \zeta(s) \{2 - \zeta(s) [1 + \rho^2(s)]\} \approx \zeta(s) \{2 - \zeta(s)\}, \tag{30}$$

$$S_T(s, 0) = mk^{-1} \{1 - n\zeta(s) [2 - \zeta(s) (1 + \rho^2(s))]\} \approx mk^{-1} \{1 - n\zeta(s) [2 - \zeta(s)]\}. \tag{31}$$

The symmetric form for the TE in central collisions

$$S_T(s, 0) = k^{-1} [1 - \zeta(s)]^2 \tag{32}$$

derived from (31) can also be viewed as the first order approximation of the logarithm series $S_T(s, 0) = k^{-1} \ln^2 \zeta$. Thus, for exactly central pp and $\bar{p}p$ collisions, only energy dependence for $R_{e/t}$ remains, which varies in different models. Detailed analysis of this dependence for pp and for $\bar{p}p$ scattering as well as for joined sample for these collisions¹ is made in [53] with help of the fitting of experimental data by a some empirically chosen function.

In general, the asymptotic value $\zeta(s)|_{s \rightarrow \infty}$ varies from one approach to another due to model-dependent value of $R_{e/t}$ at $s \rightarrow \infty$. Result from [53], obtained with help of the asymptotic theorems and assumptions for the properties of scattering amplitude for binary process $1 + 2 \rightarrow 3 + 4$ within axiomatic quantum field theory (AQFT), assumes that $\zeta(s)|_{s \rightarrow \infty} \rightarrow 3$. Approach of the partonic disks [54] provides some faster growth of the ratio of elastic to total cross section which leads to the $R_{e/t}(s) \rightarrow 1$ at $s \rightarrow \infty$ and consequently $\zeta(s)|_{s \rightarrow \infty} \rightarrow 4$. It should be noted that $G_{\text{inel}}(s, 0)|_{s \rightarrow \infty} < 0$ in accordance with the (30) within models with $\zeta(s)|_{s \rightarrow \infty} > 2$. On the other hand, if the total cross section in the asymptotic energy domain is half one has usually today, i.e. is bounded by modified Froissart–Martin limit $\sigma_{\text{tot}}(s)|_{s \rightarrow \infty} < (\pi/2m_\pi^2) \ln^2 \varepsilon$ [55], then the inelastic cross section bounded by $(\pi/4m_\pi^2) \ln^2 \varepsilon$ is two times smaller, where m_π is the pion mass [51], $\varepsilon \equiv s/s_0$ and $s_0 = 1 \text{ GeV}^2$. Consequently $R_{e/t}(s) \rightarrow 1/2$ at $s \rightarrow \infty$. Furthermore the harder boundary result $R_{e/t}(s)|_{s \rightarrow \infty} < 1/2$ can be obtained if it is accepted that the elastic cross section cannot be larger than the inelastic cross section (σ_{inel}), the limiting case being an expanding black disk [56]. These allow the restoration of $\zeta(s)$ into the interval $(0, 2)$. However, if the modified Froissart–Martin limit [55] is

¹ Below for brevity the joined sample is also called the ensemble for nucleon-nucleon scattering.

exceeded and / or $\sigma_{\text{el}} > \sigma_{\text{inel}}$ can be at $s \rightarrow \infty$, then in such approaches the identification of the inelastic overlap function with some probability requires additional study and justification at asymptotic energies².

The experimental database for $R_{e/t}(s)$ and fit results for this quantity are taken from [53] and are used in order to evaluate the energy dependencies for both $G_{\text{inel}}(s, 0)$ and $S_T(s, 0)$ in pp , $\bar{p}p$ scattering³. Among analytic functions suggested in [53] the approximation with the power law term $\propto \varepsilon^{-\beta}$ leads to the slightly better description of experimental data for $R_{e/t}$ than the function with the term $\propto \ln^{-\gamma} \varepsilon$ at low boundaries for fitted intervals on energy $\sqrt{s_{\text{min}}} \geq 3$ GeV. According to the discussion above, the approximate relations in (30) and (31) are valid for $\sqrt{s} \gtrsim 5$ (3) GeV for pp ($\bar{p}p$) collisions at accuracy level not worse than 0.09 (0.04). Consequently, the following analytic function is considered for $R_{e/t}(s)$:

$$R_{e/t}(s) = a_1 + a_2 \ln^{a_3} \varepsilon + a_4 \varepsilon^{-a_5}, \quad (33)$$

where free parameters a_i , $i = 1 - 5$ depended on range of the fit, i.e., on the low boundary for energy interval $s \geq s_{\text{min}}$ [53]. Moreover, the results from [53] allow the comparison with other phenomenological approaches: the smooth curves for $G_{\text{inel}}(s, 0)$ and $S_T(s, 0)$ are obtained by using the $R_{e/t}(s)$ estimated as the ratio of approximation for σ_{el} from [57] to "standard" functions for σ_{tot} in pp and $\bar{p}p$ reactions from [51].

Figs. 1 and 2 show the energy dependence for the inelastic overlap function in central pp and $\bar{p}p$ collisions, respectively. Estimations for $G_{\text{inel}}(s, 0)$, deduced with help of the experimental values for $R_{e/t}(s)$, are shown by points. Smooth curves obtained in [53] are also re-calculated for $G_{\text{inel}}(s, 0)$. In general, the experimental estimations are characterized by large errors which makes it difficult to obtain unambiguous physical conclusions. Considering large errors one can suppose that the pp (Fig. 1) and the $\bar{p}p$ scattering (Fig. 2) are close to the black disk picture at $\sqrt{s} \lesssim 10$ GeV. Then, trend is seen to some decreasing of $G_{\text{inel}}(s, 0)$ up to the the highest Intersecting Storage Rings (ISR) energy $\sqrt{s} \approx 63$ GeV. There are gaps without experimental data for both pp and $\bar{p}p$ especially large for the first case and the importance of new experimental data from Relativistic Heavy Ion Collider (RHIC) at $\sqrt{s} \sim 0.1 - 0.5$ TeV and from low-energy Large Hadron Collider (LHC) mode at $\sqrt{s} \sim 1.0$ TeV is mentioned elsewhere [53]. Experimental estimations for pp at $\sqrt{s} > 1$ TeV agree quite well with black disk picture (Fig. 1, inner panel) and this statement is valid for $\bar{p}p$ starting with $\sqrt{s} = 546$ GeV (Fig. 2). As seen in Figs. 1, 2 the smooth curves obtained within various models describe reasonably of experimental estimations for the $G_{\text{inel}}(s, 0)$ in whole available energy range $\sqrt{s} \geq 5$ (3) GeV for pp ($\bar{p}p$) collisions. This is expected due to corresponding results for $R_{e/t}(s)$ [53]. The constant $G_{\text{inel}}(s, 0) \approx 1.0$ agrees with high-energy pp and $\bar{p}p$ experimental estimations. Empirical curve based on the (33) is close to the one obtained with parameterizations from [51, 57] at $\sqrt{s} \leq 1$ TeV for both pp (Fig. 1) and $\bar{p}p$ (Fig. 2) collisions. In the last case some discrepancy is seen at $\sqrt{s} \lesssim 10$ GeV which can be explained by the fact that, strictly speaking, the parametrization for σ_{el} from [57] is obtained at $\sqrt{s} \geq 10$ GeV. For pp scattering both curves based on the (33) and on the parameterizations from [51, 57] show gradual decrease of the $G_{\text{inel}}(s, 0)$ at ultra-high energies $\sqrt{s} \gtrsim 100$ TeV and (33) leading to the noticeable deviation from black disk limit at $\mathcal{O}(100 \text{ TeV})$. In general, this observation is also valid for $\bar{p}p$ (Fig. 2). However, in this case the behavior of the curves is characterized by considerable uncertainty in multi-TeV energy domain $\sqrt{s} > 10$ TeV due to lack of the experimental estimations.

Fig. 3 shows the $G_{\text{inel}}(s, 0)$ for nucleon-nucleon collisions. The experimental estimations agree for pp and $\bar{p}p$ scattering at close \sqrt{s} . The constant describe points reasonably at intermediate energies $10 \leq \sqrt{s} \leq 100$ GeV and for high-energy domain. One can note that the constant dotted line obtained with help of the corresponding result for $\sqrt{s} > 1$ TeV from [53] agree quite well with experimental estimation at smaller $\sqrt{s} = 546$ GeV. Then, one can suggest that the constant allow the reasonable description of the experimental estimations to $G_{\text{inel}}(s, 0)$ for joined nucleon-nucleon sample in wider energy range $\sqrt{s} > 100$ GeV with respect to the result for $R_{e/t}(s)$ [53]. The approach based on the (33) predicts the onset of deviation from the black disk limit at $\mathcal{O}(100 \text{ TeV})$ and the continues decrease of the inelastic overlap function in central nucleon-nucleon collisions with growth of s provides $G_{\text{inel}}(s, 0) \rightarrow 0$ at PeV energies.

Taking into account the analysis in [16] the TE in central pp , $\bar{p}p$ collisions is calculated at $\sqrt{s_c} = 25.0$ GeV in present work. As seen from (32) the $\zeta(s) = 1.0$ corresponds to a maximum ($s < s_c$) or a minimum ($s > s_c$) of the $S_T(s, 0)$. Results from [53] show the $\zeta(s) \approx 1.0$ can be reached in separate points at intermediate energies $\sqrt{s} \simeq 5$ GeV and this is a characteristic value in TeV energy domain. Detailed analysis of the (32) shown that $S_T(s, 0)$ demonstrates the sharper behavior as the s approaches to the critical value s_c . Furthermore, the absolute values of the TE for

² Usually the phenomenological models consider the energy domain no wider than $\sqrt{s} \gtrsim 3 - 5$ GeV excluding the narrow range on s close to the low-energy boundary $s_{\text{l.b.}} \equiv 4m_p^2$ for the interactions (pp , $\bar{p}p$) under discussion in which $R_{e/t}$ reaches large values in pp , where m_p is the proton mass [51]. Moreover, this low-energy range is excluded in the present analysis due to above condition $|\rho(s)| \lesssim 0.3$.

³ In the paper total errors are used for estimations based on the experimental points for $R_{e/t}(s)$ unless otherwise specified. The total error is calculated as addition of systematic and statistical uncertainties in quadrature [51].

$s < s_c$ ($|S_T| = -S_T$) are mostly larger by orders than that for $s \gg s_c$ ($|S_T| = S_T$) at $\sqrt{s_c} = 25.0$ GeV. Therefore, the $|S_T(s, 0)|$ seems more adequate quantity for study of s -dependence in wide energy domain for the symmetric form of the TE in central pp , $\bar{p}p$ collisions.

Figs. 3 – 6 show the energy dependence of the magnitude of the TE in central pp , $\bar{p}p$ collisions and for joined sample in nucleon-nucleon scattering, respectively. Experimental estimations for $|S_T(s, 0)|$ are deduced with help of the database for $R_{e/t}(s)$ [53] and relations (25), (32). Notations for experimental estimations and smooth curves are the same as in Figs. 1 – 2. Different collisions are characterized by similar values of $|S_T(s, 0)|$, the maximum value $|S_T(s, 0)|_{sim1}$ is reached for experimental estimations obtained close to the critical energy $\sqrt{s_c}$ (Figs. 4, 6) and growth of s leads to the fast decreasing of $|S_T(s, 0)|$ at $s > s_c$. The empirical curves based on the (33) and on the parameterizations from [51, 57] demonstrate the sharp deeps at TeV energies and these deeps are at various s in pp (Fig. 4) while they coincide in $\bar{p}p$ scattering (Fig. 5). The parameterizations from [51, 57] provides $|S_T(s, 0)|$ mostly large than the empirical function (33) at low and intermediate energies $s < s_c$ in both pp and $\bar{p}p$ collisions. The situation is more ambiguous at high energies $\sqrt{s} > 1$ TeV. For the first case (Fig. 4), the curve evaluated from (33) lies higher than the curve based on the parameterizations from [51, 57] up to the $\sqrt{s} \simeq 5$ TeV and in the ultra-high energy domain $\sqrt{s} \gtrsim 100$ TeV. In $\bar{p}p$ scattering (Fig. 5), the fit result from [53] provide smooth curve for $|S_T(s, 0)|$ which is higher than the similar curve deduced with help of the functions from [51, 57] and difference is especially visible at $\sqrt{s} \geq 10$ TeV.

V. FINAL REMARKS

As pointed out in [16], the total cross section experimental dataset to pp and $\bar{p}p$ present two fractal dimensions. The Peres–Shmerkin theorem [58] states that if a dataset possesses two fractal dimensions, then the sum of both is not equal to the original dimension of the dataset [17]. The fundamental question is if the total cross section forms a closed, has no isolated points, dense and compact dataset. Of course, the dataset is dense since the general belief is that it can be described by a continuous real-valued function of s , for instance. It is compact and has no isolated point as well. However, the term closed implies the existence of a maximum value to the total cross section rise. Note that the Froissart–Martin bound does not prevent this behavior but one cannot assume this from the approach used here.

As noted in [33–35] the region near the central collision ($b = 0$ fm) presents a growing gray area indicating a tendency at higher energies, corroborated by [59, 60]. Moreover, the inelastic overlap function is well-described only by the use of at least two Gaussian [60]. This behavior on the impact parameter space may be viewed as a reflex of the occurrence of fractal dimensions in energy and momentum spaces [16–23]. Therefore, the inelastic overlap function may also present a fractal behavior at each s considered, indicating a phase transition occurring at $b_0 = b(s_c)$, where b_0 is given by the zero of the confinement potential as well as by the temperature function obtained here.

The principle of maximum entropy states that the probability function *correctly* describing a dataset is the one with the largest entropy S . The entropy (12) is about a particular scattering at some fixed- s . To each s_i one can construct a dataset taking the pair $[0, G_{inel}(s_i, b(s_i))]$, i.e., the line contained in $[0, b(s_i)]$. The dataset thus constructed is a homeomorphism to the Cantor set and then, the Peres–Shmerkin theorem is valid since the dataset formed possess two fractal dimensions. Therefore, by the approach used here the precise knowledge of whole $G_{inel}(s, b)$ is avoided by the Peres–Shmerkin theorem and the black disk limit may be reduced to a quasi-black disk limit near $b = 0$ (the gray disk in [33, 34]). This result is independent of the total cross-section reach a maximum or not.

The TE (12) can also be related to the amount of information in the area of width k^{-1} and the curve given by $m[1 - nG_{inel}(s, b)]$ depending on each s used. Of course, $m[1 - nG_{inel}(s, b)]$ is limited to the range $\forall i : [0, G_{inel}(s_i, b(s_i))]$, and, therefore, this area assumes a finite value as well as the amount of information one can obtain from it.

The study of the transition point (the critical temperature) can reveal some important properties of the arrangement of the internal constituents [61]. The temperature at the transition point s_c is, of course, of great interest and the result obtained here show the possibility of negative temperatures occurrence inside the hadron in both energy regimes $s < s_c$ and $s > s_c$. In the first case, the negative temperature allows to hadron the formation of a torus with a smoothed edge toward the center. The latter, indicate the hadron acquires a disk-like shape, tending to a point-like object as the energy tends to infinity. As well-known, the negative temperature has been interpreted as the change in the occupancy of the energy states [11] along the years: the probability of the occupation of the higher-energy states is greater than the lower-energy states. Therefore, the phase transition obtained here is evidenced by an inversion of the occupation number of the energy states by the internal constituents of the hadron as the energy increases. The negative temperature also avoids the internal constituents to gain kinetic energy, turning the system stable [64].

The Hagedorn temperature in its first beginning was thought as the highest possible temperature to the hadronic matter [46]. However, it was shown later that this temperature is, in fact, a critical temperature to the phase transition [62] from the hadronic matter to a quark-gluon plasma. The model presented here indicates a phase transition

occurring at $b_0 = b(s_c)$ for both energy regimes where the hadron suddenly changes its internal configuration in the energy occupation states of its internal constituents. In the asymptotic energy regime, the critical value b_0 shrinks to zero. Besides, if the majority of the quarks and gluons are located in the region $b < b_0$, then the energy density grows and the higher-energy occupation states must tend to maximum, may be related with the dynamics flavor [63]. Moreover, this growth also implies in the rise of the total cross section as $s \rightarrow \infty$.

The use of the Coulomb or the confinement potential cannot allow one to obtain a precise indication of the critical point. However, the approach adopted here may be used as a first glance to improve the theoretical understanding of pp and $\bar{p}p$ collision processes.

The phenomenological analysis for the inelastic overlap function and for the magnitude of the TE in central collisions allows the following conclusions. The $G_{\text{inel}}(s, 0)$ is close to the black disk limit at $\sqrt{s} \lesssim 5$ GeV and especially at TeV energies in both pp and $\bar{p}p$ collisions. There is indication on the $G_{\text{inel}}(s, 0) < 1$ within large errors in the region $10 \lesssim \sqrt{s} \lesssim 100$ GeV. Smooth curves evaluated with help of the model-independent empirical function (33) and from parameterizations with universal $\ln^2 \varepsilon$ asymptotic term for σ_{tot} , σ_{el} show the deviation of $G_{\text{inel}}(s, 0)$ from the black disk limit at ultra-high energies. The curve based on the model-independent approach predicts $G_{\text{inel}}(s, 0) \rightarrow 0$ in nucleon-nucleon collisions at PeV energies. The experimental estimations for magnitude of the TE reaches the maximum $|S_T(s, 0)| \sim 1$ close to the critical energy and smooth curves predict very small values of $|S_T(s, 0)|$ for nucleon-nucleon collisions at ultra-high energies, in particular, $|S_T(s, 0)| \sim 10^{-10}$ at $\sqrt{s} \sim 1$ PeV in accordance with the model-independent curve based on the equation (33).

Acknowledgments

S.D.C. and C.V.M. thanks to UFSCar by the financial support. The work of V.A.O. was supported partly by NRNU MEPhI Academic Excellence Project (contract No 02.a03.21.0005 on 27.08.2013).

-
- [1] S. Sachdev, *Quantum Phase Transitions*. Cambridge Univ. Press (2011).
 - [2] M. E. Fisher, Rep. Prog. Phys. **30**, 615 (1967).
 - [3] L. D. Landau and E. M. Lifshitz, *Statistical physics. Part 1*. Elsevier (1980).
 - [4] V. L. Berezinskii, Zh. Eksp. Teor. Fiz. **59**, 907 (1970) [Sov. Phys. JETP **32**, 493 (1971)].
 - [5] J. M. Kosterlitz and D. J. Thouless, J. Phys. C **6**, 1181 (1973).
 - [6] C. Tsallis, J. Stat. Phys. **52**, 479 (1988); *Introduction to Nonextensive Statistical Mechanics: Approaching a Complex World*. Springer Science (2009).
 - [7] C. E. Shannon, Bell S. Tech. J. **27**, 379 (1948).
 - [8] A. Rényi, Proceedings of the IV Berkeley Symposium on Mathematics, Statistics and Probability, p. 547 (1960).
 - [9] I. Bengtsson and K. Zyczkowski, *Geometry of Quantum States: An Introduction to Quantum Entanglement*. Cambridge Univ. Press (2006).
 - [10] C. Beck, arXiv: 0902.1235v2 [cond-mat.stat-mech] (2009).
 - [11] L. del Rio et al., Nature **474**, 61 (2011).
 - [12] H. Foroozand and S. V. Weijs, Entropy **19**, 520 (2017).
 - [13] E. Jiménez, N. Recalde, and E. J. Chacón, Entropy **19**, 293 (2017).
 - [14] I. Zborovský and M. V. Tokarev, Int. J. Mod. Phys. A **24**, 1417 (2009).
 - [15] I. V. Vancea, Int. J. Mod. Phys. A **23**, 4485 (2008).
 - [16] F. S. Borcsik and S. D. Campos, Mod. Phys. Lett. A **31**, 1650066 (2016).
 - [17] V. A. Okorokov and S. D. Campos, Int. J. Mod. Phys. A **32**, 1750175 (2017).
 - [18] A. Bialas, Nucl. Phys. A **545**, 285c (1992).
 - [19] A. Bialas, Acta Phys. Polon. B **23**, 561 (1992).
 - [20] N. G. Antoniou, F. Diakonou and C. G. Papadopoulos, Phys. Lett. B **265**, 399 (1991).
 - [21] N. G. Antoniou, V. E. Zambetakis, F. K. Diakonou, and N. K. Diakonou, Z. Phys. C **55**, 631 (1992).
 - [22] N. G. Antoniou, F. Diakonou, I. S. Mistakidis, and C. G. Papadopoulos, Phys. Rev. D **49**, 5789 (1994).
 - [23] N. G. Antoniou, N. Davis, and F. K. Diakonou, Phys. Rev. C **93**, 014908 (2015).
 - [24] A. Deppman, Phys. Rev. D **93**, 054001 (2016).
 - [25] F. S. Navarra, O. V. Utyuzh, G. Wilk, and Z. Włodarczyk, Phys. Rev. D **67**, 114002 (2003).
 - [26] V. Čápek and D. P. Sheehan *Challenges to the Second Law of Thermodynamics: Theory and Experiment*. Springer (2005).
 - [27] L. Van Hove, Rev. Mod. Phys. **36**, 655 (1964).
 - [28] P. D. B. Collins, *An Introduction to Regge Theory and High Energy Physics*. Cambridge Univ. Press (1977).
 - [29] V. Barone and E. Predazzi, *High-Energy Particle Diffraction*. Springer (2002).
 - [30] S. D. Campos, Int. J. Mod. Phys. A **25**, 1937 (2010).

- [31] N. A. Amos et al. (E710 Collaboration), Phys. Lett. B**247**, 127 (1990); F. Abe et al. (CDF Collaboration), Phys. Rev. D**50**, 5518 (1994).
- [32] G. Antchev et al. (TOTEM Collaboration), Europhys. Lett. **96**, 21002 (2011).
- [33] I. M. Dremin, Phys. Uspekhi **58**, 61 (2015).
- [34] I. M. Dremin, Phys. Uspekhi **60**, 333 (2017).
- [35] W. Broniowski and E. Ruiz Arriola, Acta Phys. Polon. B Proc. Supp., **10**, 1203 (2017).
- [36] A. Alkin, E. Martinov, O. Kovalenko, and S. M. Troshin, Phys. Rev. D**89**, 091501 (2014).
- [37] V. V. Anisovich, V. A. Nikonov, and J. Nyiri, Phys. Rev. D**90**, 074005 (2014).
- [38] S. M. Troshin and N. E. Tyurin, Int. J. Mod. Phys. A**29**, 1450151 (2014).
- [39] V. V. Anisovich, Phys. Uspekhi **58**, 1043 (2015).
- [40] S. N. Troshin and N. E. Tyurin, Mod. Phys. Lett. A**31**, 1650079 (2016).
- [41] J. L. Albacete and A. Soto-Ontoso, Phys. Lett. B**770**, 149 (2017).
- [42] E. Ruiz Arriola and W. Broniowski, Phys. Rev. D**95**, 074030 (2017).
- [43] H. Cheng and T. T. Wu, Phys. Rev. Lett. **24**, 145 (1970).
- [44] W. Heisenberg, Z. Phys. **133**, 65 (1952).
- [45] G. Rotundo and M. Ausloos. Eur. Phys. J. B**86**, 169 (2013).
- [46] R. Hagedorn, Nuovo Cim. Suppl. **3**, 147 (1965); Nuovo Cim. **56A**, 1027 (1968).
- [47] I. M. Dremin, arXiv: 1511.03212 [hep-ph] (2015).
- [48] S. D. Campos and V. A. Okorokov, arXiv: 1807.02061 [hep-ph] (2018).
- [49] M. Kaufman, *Principles of Thermodynamics*. Marcel Dekker, Inc. (2001).
- [50] A. V. Smilga, Phys. Rept. **291**, 1 (1997).
- [51] C. Patrignani et al. (Particle Data Group), Chin. Phys. C**40**, 100001 (2016).
- [52] N. F. Ramsey, Phys. Rev. **103**, 10 (1956).
- [53] V. A. Okorokov, arXiv: 1805.10514 [hep-ph] (2018).
- [54] V. V. Anisovich, Phys. Uspekhi, **58**, 963 (2015).
- [55] A. Martin, Phys. Rev. D**80**, 065013 (2009).
- [56] A. Martin and S. M. Roy, Phys. Rev. D**91**, 076006 (2015).
- [57] G. Antchev *et al.* (TOTEM Collaboration), arXiv: 1712.06153 [hep-ex] (2017).
- [58] Y. Peres and P. Shmerkin, Erg. Theor. Dynam. Syst. **29**, 201 (2009).
- [59] A. K. Kohara, E. Ferreira, and T. Kodama, arXiv: 1408.1599 [hep-ph] (2014).
- [60] D. A. Fagundes, M. J. Menon and P. V. R. G. Silva, Nucl. Phys. A**946**, 194 (2016).
- [61] J. I. Kapusta and K. A. Olive, Nucl. Phys. A**408**, 478 (1983).
- [62] N. Cabibbo and G. Parisi, Phys. Lett. B**59**, 67 (1975).
- [63] T. Albash, V. G. Filev, C. V. Johnson, and A. Kundu, Phys. Rev. D**77**, 066004 (2008).
- [64] S. Braun *et al.*, Science **339**, 52 (2013).

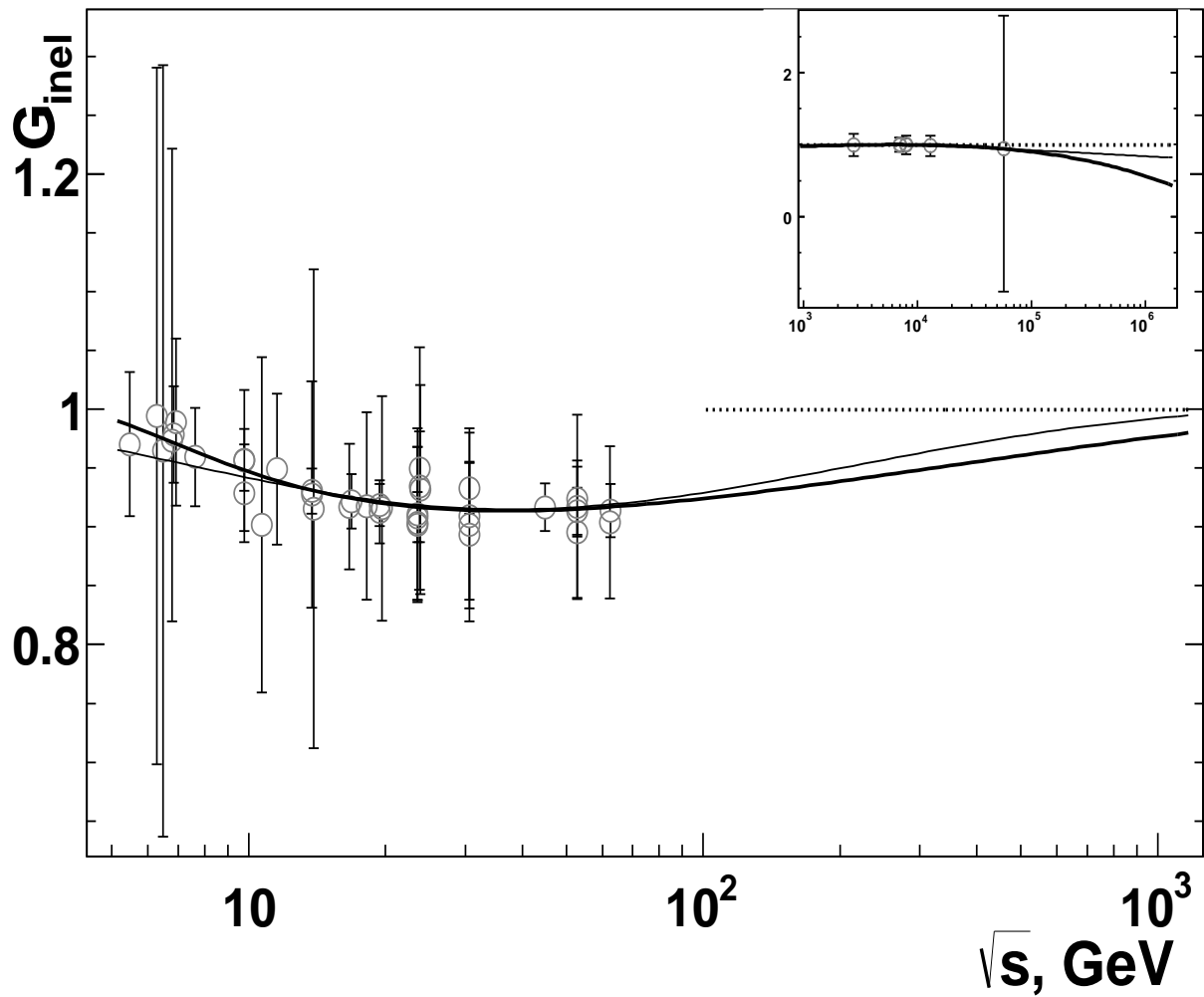


FIG. 1: Energy dependence for the inelastic overlap function in central pp collisions $G_{\text{inel}}(s, 0)$. Experimental estimations are shown by points, curves are evaluated with help of the smooth dependencies for $R_{e/t}^{pp}$ from [53]. Solid curve corresponds to the results of the fitting of experimental $R_{e/t}^{pp}(s)$ by (33) at $\sqrt{s_{\text{min}}} = 5$ GeV and dotted line – by constant at $\sqrt{s_{\text{min}}} = 100$ GeV (see detailed description in the text). The thin solid line is obtained on basis of the ratio of the approximation for $\sigma_{\text{el}}(s)$ from [57] to the analytic function for $\sigma_{\text{tot}}^{pp}(s)$ from [51]. Inner panel: experimental estimations and curves for the energy domain $\sqrt{s} > 1$ TeV.

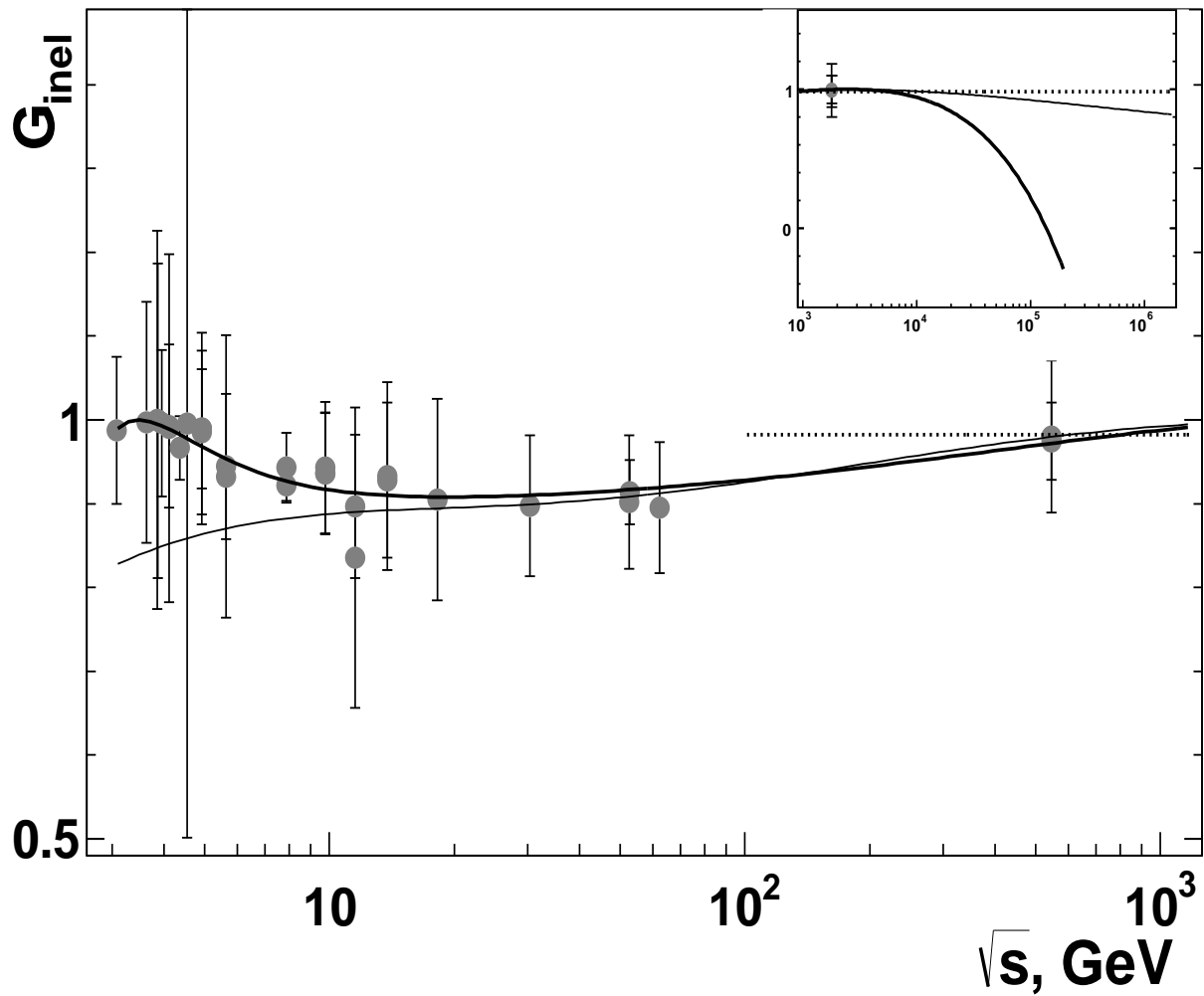


FIG. 2: Energy dependence for the inelastic overlap function in central $\bar{p}p$ collisions $G_{\text{inel}}(s, 0)$. Experimental estimations are shown by points, curves are evaluated with help of the smooth dependencies for $R_{e/t}^{\bar{p}p}$ from [53]. Solid curve corresponds to the results of the fitting of experimental $R_{e/t}^{\bar{p}p}(s)$ by (33) at $\sqrt{s_{\text{min}}} = 3$ GeV and dotted line – by constant at $\sqrt{s_{\text{min}}} = 100$ GeV (see detailed description in the text). The thin solid line is obtained on basis of the ratio of the approximation for $\sigma_{\text{el}}(s)$ from [57] to the analytic function for $\sigma_{\text{tot}}^{\bar{p}p}(s)$ from [51]. Inner panel: experimental estimations and curves for the energy domain $\sqrt{s} > 1$ TeV.

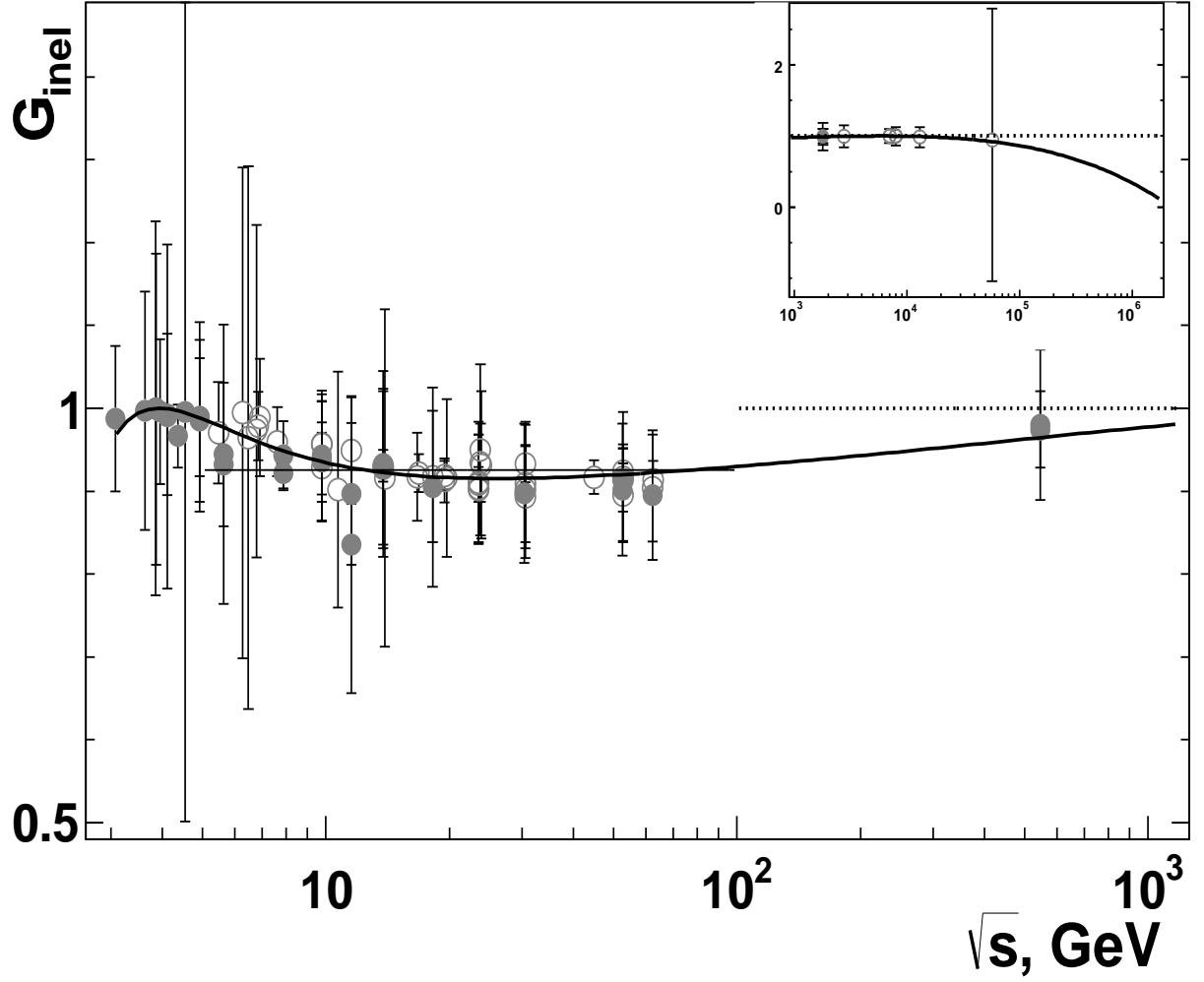


FIG. 3: Energy dependence for the inelastic overlap function in central nucleon-nucleon collisions $G_{\text{inel}}(s, 0)$. Experimental estimations are shown by open points for pp and by solid points for $\bar{p}p$ scattering, curves are evaluated with help of the smooth dependencies for $R_{e/t}$ from [53]. Solid curve corresponds to the results of the fitting of experimental sample for $R_{e/t}(s)$ joined for pp and $\bar{p}p$ by (33) at $\sqrt{s_{\text{min}}} = 3$ GeV, dotted line – by constant at $\sqrt{s_{\text{min}}} = 1$ TeV, thin solid curve corresponds the fit of $R_{e/t}$ by constant in the intermediate energy range at $\sqrt{s} \in [10; 100]$ GeV (see detailed description in the text). Inner panel: experimental estimations and curves for the energy domain $\sqrt{s} > 1$ TeV.

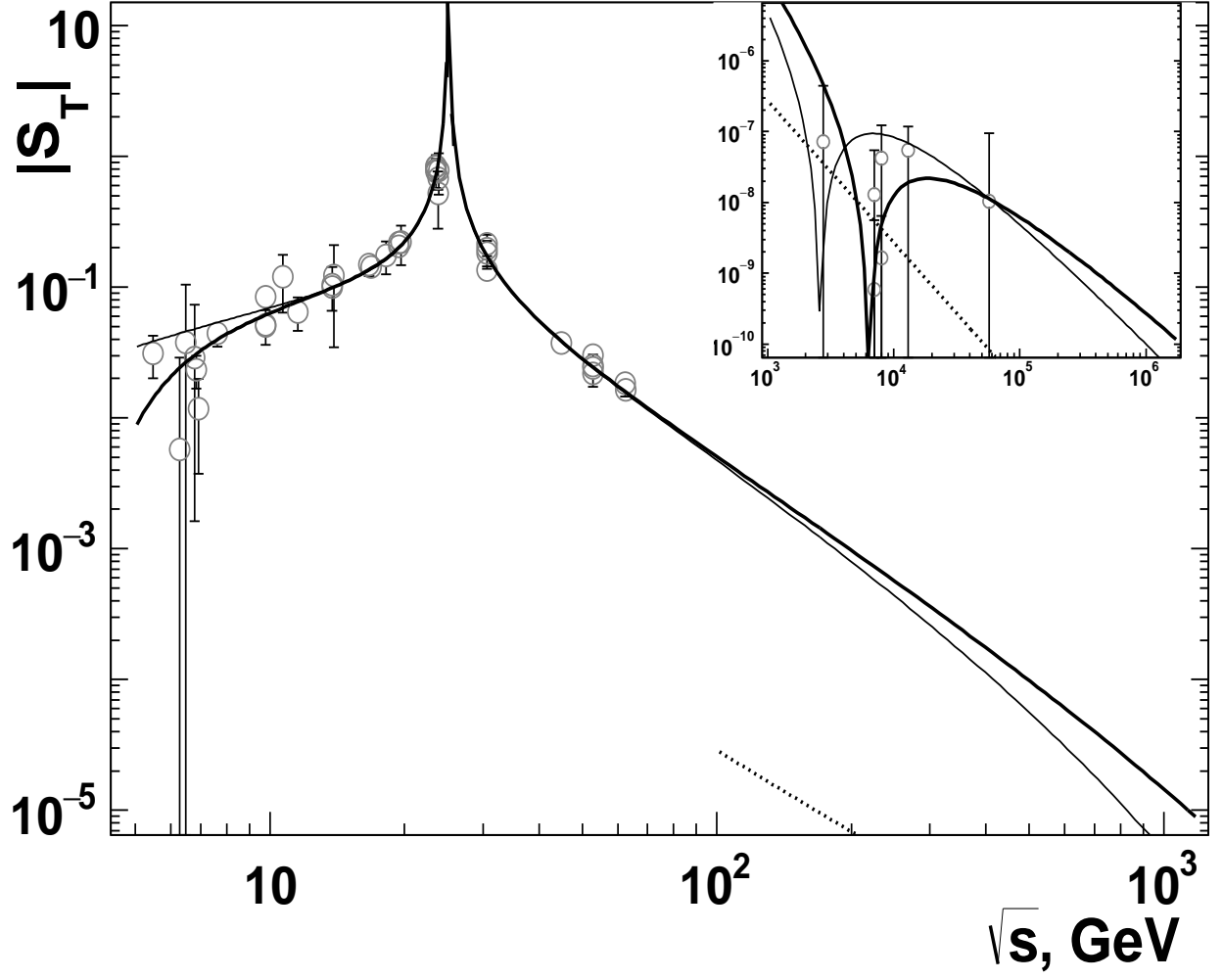


FIG. 4: Energy dependence for absolute values of the TE in central pp collisions $S_T(s, 0)$. Notations for experimental estimations and curves are the same as in Fig. 1. Inner panel: experimental estimations and curves for the energy domain $\sqrt{s} > 1$ TeV.

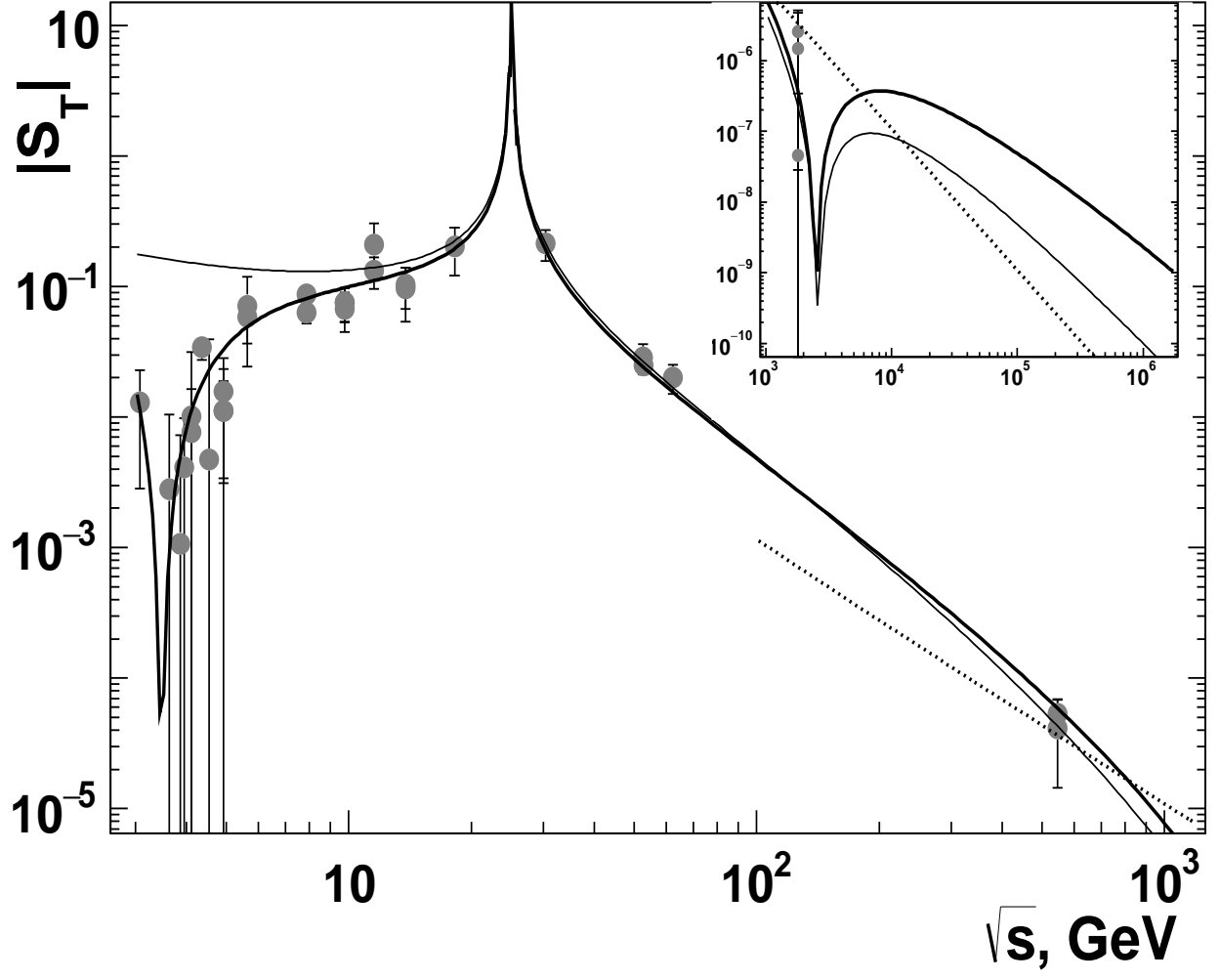


FIG. 5: Energy dependence for absolute values of the TE in central pp collisions $S_T(s, 0)$. Notations for experimental estimations and curves are the same as in Fig. 2. Inner panel: experimental estimations and curves for the energy domain $\sqrt{s} > 1$ TeV.

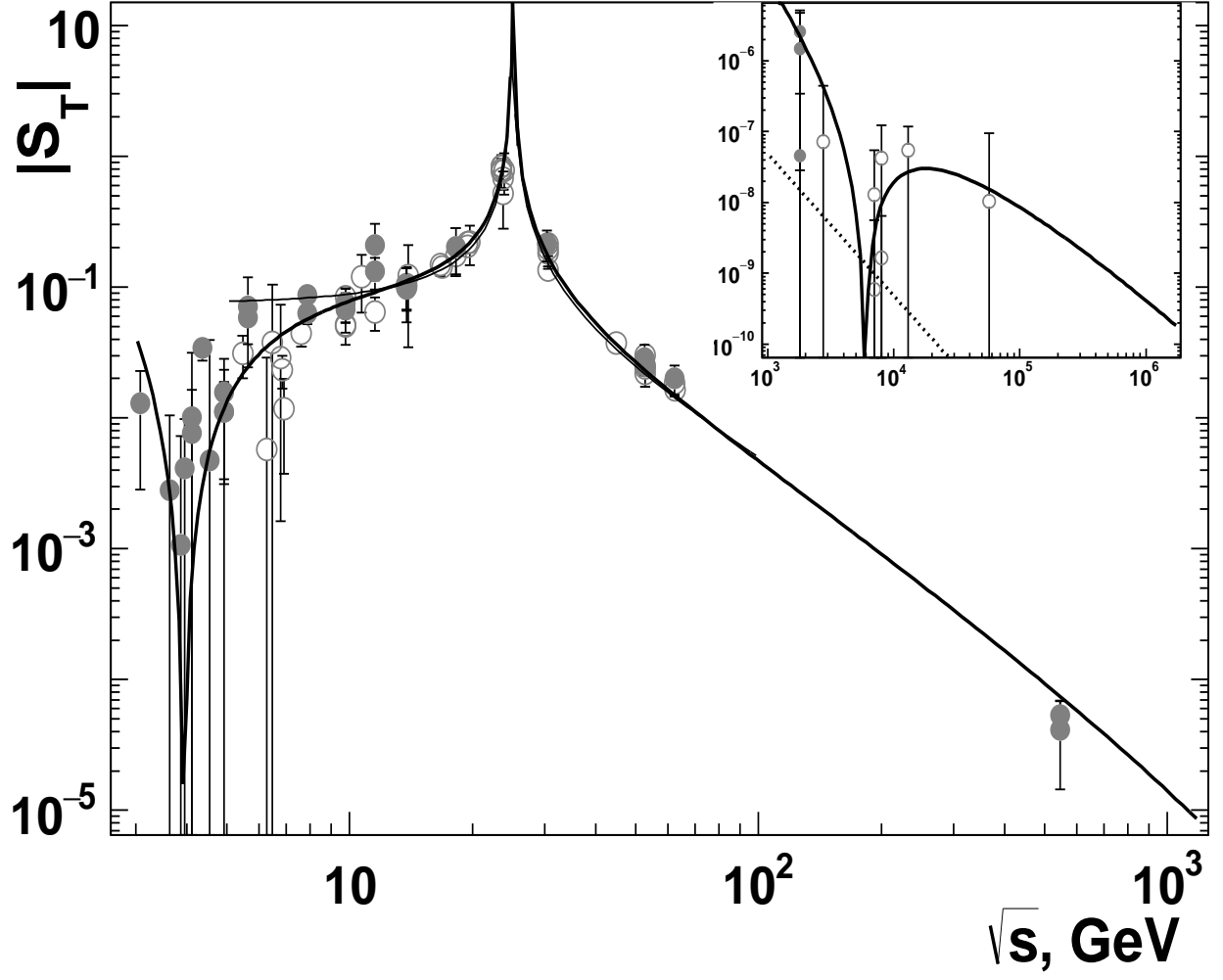


FIG. 6: Energy dependence for absolute values of the TE in central pp collisions $S_T(s, 0)$. Notations for experimental estimations and curves are the same as in Fig. 1. Inner panel: experimental estimations and curves for the energy domain $\sqrt{s} > 1$ TeV.